Particle path tracking method in two- and three-dimensional continuously rotating detonation engines

Zhou Rui(周 蕊)†, Wu Dan(武 丹), Liu Yan(刘 岩), and Wang Jian-Ping(王健平)

State Key Laboratory of Turbulence & Complex Systems, Center for Applied Physics and Technology, Department of Mechanics and Engineering Science, College of Engineering, Peking University, Beijing 100871, *China*

(Received 21 February 2014; revised manuscript received 27 May 2014; published online 10 October 2014)

The particle path tracking method is proposed and used in two-dimensional (2D) and three-dimensional (3D) numerical simulations of continuously rotating detonation engines (CRDEs). This method is used to analyze the combustion and expansion processes of the fresh particles, and the thermodynamic cycle process of CRDE. In a 3D CRDE flow field, as the radius of the annulus increases, the no-injection area proportion increases, the non-detonation proportion decreases, and the detonation height decreases. The flow field parameters on the 3D mid annulus are different from in the 2D flow field under the same chamber size. The non-detonation proportion in the 3D flow field is less than in the 2D flow field. In the 2D and 3D CRDE, the paths of the flow particles have only a small fluctuation in the circumferential direction. The numerical thermodynamic cycle processes are qualitatively consistent with the three ideal cycle models, and they are right in between the ideal F–J cycle and ideal ZND cycle. The net mechanical work and thermal efficiency are slightly smaller in the 2D simulation than in the 3D simulation. In the 3D CRDE, as the radius of the annulus increases, the net mechanical work is almost constant, and the thermal efficiency increases. The numerical thermal efficiencies are larger than F–J cycle, and much smaller than ZND cycle.

Keywords: continuously rotating detonation engine, thermodynamic cycle, numerical simulation, particle path tracking method

PACS: 47.40.Rs, 47.40.–x **DOI:** 10.1088/1674-1056/23/12/124704

1. Introduction

The detonation has an inherently higher thermodynamic efficiency than the constant-pressure deflagration.[1–3] In recent years, the continuously rotating detonation engines (CRDEs) based on detonation have been extensively studied. In the CRDE, the detonation is initiated in a cylindrical channel chamber, and it propagates along the circumferential direction, which is perpendicular to the direction of fuel injection. The detonation wave can continuously propagate over a wide range of injection velocities and does not need repetitive ignition. These characteristics can possibly greatly reduce the difficulties in developing a detonation engine.

Both Wolanski[4] and Lu *et al.*[5] gave the comprehensive reviews of CRDE. Voitsekhovskii[6] initially proposed the concept of CRDE and achieved a brief continuous detonation of premixed acetylene and ethylene in a circular tube. Theoretical analyses and preliminary experimental research on the application of the rotating detonations to rocket propulsion were first conducted by Adamson and Olsson[7] and Nicholls *et al.*[8] More recently, successful experimental research and comprehensive numerical simulation analysis on CRDE have been performed in Russia,[9,10] Poland,[11] France,[12,13] USA,[14] China,[15–20] and Japan.[21,22] In our group, Shao and Wang[15,16] and Shao *et al.*[17] comprehensively performed the three-dimensional (3D) numerical simulations on CRDE. They demonstrated the multiple cycles of rotating detonation, and discussed several key issues, including the fuel injection limitation, self-ignition, thrust performance, and nozzle effects.

So far, there has been little research, either numerical or experimental, on the thermodynamic performance of CRDE. Most of the previous numerical simulation studies have focused on the overall description of the flow-field within CRDE chamber. In the previous work, we have proposed the particle path tracking method to analyze the two-dimensional (2D) CRDE flow field and described its thermodynamic properties.[18] The paths of flow particles were tracked, and the effects of the detonation wave, the oblique shock wave, and the contact surface on path and flow parameter were investigated. The corresponding p–v and T–s diagrams could then be used to calculate the net mechanical work and thermal efficiency. In the present paper, the particle path tracking method is further used in the 2D and 3D numerical simulations. We focus on the movement of the flow particles, and the comparison among the flow field parameters on the different annuli in the 3D CRDE combustion chamber. The flow field parameters, the particle paths, and the thermodynamic cycle processes obtained by the 2D and 3D numerical simulations are compared in detail. The corresponding p–v and T–s diagrams obtained by the simulations are compared with those obtained from the ideal Humphrey, F–J, and ZND cycle models.

†Corresponding author. E-mail: ameliazhr@163.com

© 2014 Chinese Physical Society and IOP Publishing Ltd

2. Numerical method and physical model

The 3D Euler equations are used with Korobeinikov and Levin's[23] two-step chemical reaction model of stoichiometric hydrogen/oxygen mixture. Viscosity, thermal conduction and mass diffusion are ignored. Generalized coordinates are used for transforming the curved grids in physical space into rectangular grids in the computational space. The governing equation in generalized coordinates is

$$\frac{\partial \boldsymbol{U}}{\partial t}+\frac{\partial \boldsymbol{E}}{\partial \xi}+\frac{\partial \boldsymbol{E}}{\partial \eta}+\frac{\partial \boldsymbol{G}}{\partial \zeta}=\boldsymbol{S}, \tag{1}$$

where the dependent variable vector $\boldsymbol{U}$, convective flux vectors $\boldsymbol{E}$, $\boldsymbol{F}$, and $\boldsymbol{G}$, and source vector $\boldsymbol{S}$ are defined as

$$\begin{aligned}
\boldsymbol{U} &= \frac{1}{J}[\rho\ \ \rho u\ \ \rho v\ \ \rho w\ \ e\ \ \rho\beta\ \ \rho\alpha]^{\mathrm{T}},\\
\boldsymbol{E} &= [\rho\bar{U}\ \ \rho\bar{U}u+p\xi_x\ \ \rho\bar{U}v+p\xi_y\ \ \rho\bar{U}w+p\xi_z\\
&\quad \bar{U}(p+e)\ \ \rho\bar{U}\beta\ \ \rho\bar{U}\alpha]^{\mathrm{T}},\\
\boldsymbol{F} &= [\rho\bar{V}\ \ \rho\bar{V}u+p\eta_x\ \ \rho\bar{V}v+p\eta_y\ \ \rho\bar{V}w+p\eta_z\\
&\quad \bar{V}(p+e)\ \ \rho\bar{V}\beta\ \ \rho\bar{V}\alpha]^{\mathrm{T}},\\
\boldsymbol{G} &= [\rho\bar{W}\ \ \rho\bar{W}u+p\zeta_x\ \ \rho\bar{W}v+p\zeta_y\ \ \rho\bar{W}w+p\zeta_z\\
&\quad \bar{W}(p+e)\ \ \rho\bar{W}\beta\ \ \rho\bar{W}\alpha]^{\mathrm{T}},\\
\boldsymbol{S} &= \frac{1}{J}[0\ \ 0\ \ 0\ \ 0\ \ 0\ \ \rho\dot{\omega}_\beta\ \ \rho\dot{\omega}_\alpha]^{\mathrm{T}},\\
\bar{U} &= u\xi_x+v\xi_y+w\xi_z,\\
\bar{V} &= u\eta_x+v\eta_y+w\eta_z,\\
\bar{W} &= u\zeta_x+v\zeta_y+w\zeta_z.
\end{aligned}$$

The pressure p and total energy e are calculated by using the equation of state and the energy relationship,

$$p=\rho RT, \tag{2}$$

$$e=\frac{p}{\gamma-1}+\beta\rho q+\frac{1}{2}\rho(u^2+v^2+w^2), \tag{3}$$

where ρ is the density, R the gas constant, T the temperature, γ the specific heat ratio, q the heat release per unit mass, α the reaction progress parameter in the induction period, and β the reaction progress parameter in the exothermic period. The mass production rates are obtained according to Arrhenius form:

$$\omega_\alpha = \frac{\mathrm{d}\alpha}{\mathrm{d}t}=-k_1\rho\exp(-E_1/RT), \tag{4}$$

$$\omega_\beta = \frac{\mathrm{d}\beta}{\mathrm{d}t}=\begin{cases}-k_2p^2\left[\beta^2\exp\left(\dfrac{-E_2}{RT}\right)\right.\\ \left.-(1-\beta)^2\exp\left(-\dfrac{E_2+q}{RT}\right)\right], & (\alpha=0),\\ 0, & (1>\alpha>0).\end{cases} \tag{5}$$

The parameters in Eqs. (4) and (5) are set as follows:[23] $q=4\times10^6$ J/kg, $\gamma=1.4$, $k_1=3.0\times10^8$ m^3/(kg·s), $k_2=1.04\times10^{-5}$ m^4/(N^2·s), $R=6.929\times10^2$ J/(kg·K), $E_1/q=1.71$, $E_2/q=0.347$, $E_1/R=9850$ K, $E_2/R=2000$ K.

In the numerical simulation, the spatial terms are discretized with the 5th-order MPWENO scheme,[24] and the temporal terms are discretized with the 4-step Runge–Kutta method.[25]

The combustion chamber of CRDE is a coaxial cylindrical channel. Figure 1 shows its propagation schematic diagram by numerical simulation. A detonation wave propagates circumferentially in the annular chamber while a combustible mixture is injected along the axial direction from the head end, and the burnt gas then flows out from the downstream exit. In this numerical simulation, the front section of the combustion chamber is initially filled with the premixed stoichiometric hydrogen and oxygen mixture at a pressure of 1 atm (1 atm = 1.01325×10^5 Pa) and temperature of 300 K. The other section is filled with the combustion products. After a one-dimensional (1D) C–J detonation wave is distributed in the front section near the head end to initiate the detonation, the detonation wave, leaning on the head end, propagates around the circumferential direction periodically. An oblique shock wave (marked with "5" in Fig. 1) connected with the detonation wave sweeps over the detonation product of the previous cycle.

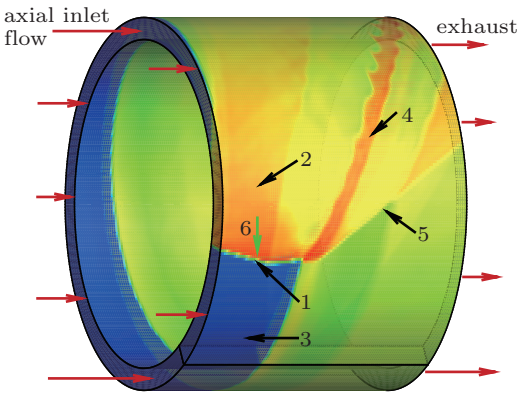


Fig. 1. (color online) CRDE propagation schematic structure. 1: detonation wave, 2: burnt product, 3: fresh premixed gas, 4: contact surface, 5: oblique shock wave, 6: detonation wave propagation direction.

In the present numerical simulation, the inlet total pressure is 3 MPa, and the ambient pressure is 0.05 MPa. At the head end, there are assumed to be a large number of Laval micro-nozzles to axially inject the premixed stoichiometric hydrogen/oxygen gas into the combustion chamber. The mass flux of the incoming fuel is controlled by the relationship between the inlet stagnation pressure and the flow pressures at the head end.[19] In the exit plane, non-reflecting outlet boundary conditions are used. Rigid wall conditions are used on the inner and outer walls. In the 2D simulation, the periodic boundary conditions are used at the upper and lower boundaries. As this study aims to investigate the CRDE's macro characteristics, rather than the micro-cell or transverse wave structure, the average grid size of 200 μm is used.

The chemical reaction model and the numerical scheme are validated in the case of 1D detonation straight tube. Stoichiometric hydrogen/oxygen mixture at 1 atm and 300 K is directly ignited by a hot spot of 30 atm and 2000 K in the 1D detonation tube. Figure 2 shows the pressure, temperature, and velocity distributions of 1D detonation. The pressure peak and temperature peak couple together tightly, showing the typical detonation structure properties. The computed propagation velocity of detonation is 2724.22 m/s, which is close to the theoretical C–J value of 2843.22 m/s obtained by using the software Gaseq. The velocity difference between the simulation and theory is less than 5%, which is caused by ignoring the changes of gas constants before and after the reaction in simulation.

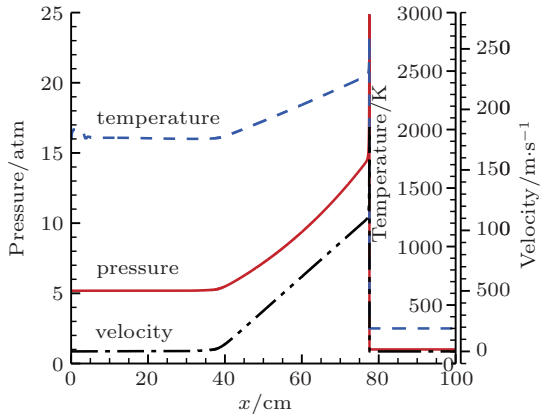


Fig. 2. (color online) Pressure, temperature, and velocity distributions of 1D detonation.

The grid dependences are tested at grid sizes of 0.05 mm, 0.1 mm, and 0.2 mm. Figure 3 shows the pressure distributions of three grid size cases. Except the Von-Neumann pressure spike, the wave structure, propagating velocity, and stable pressure after the detonation almost coincide for these three grid size cases. The above analysis proves the convergence of numerical scheme and chemical reaction model, and the grid dependence.

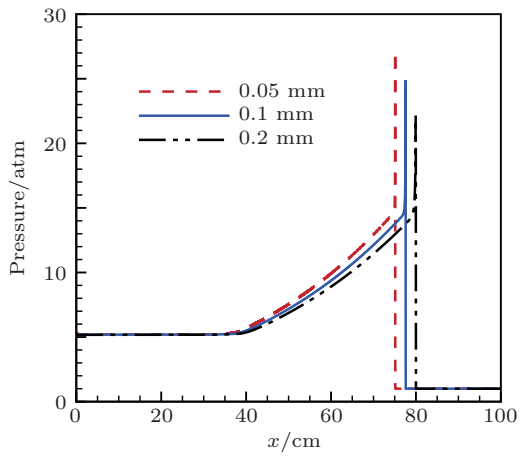


Fig. 3. (color online) Pressure distributions of 1D detonation wave propagation with three grid sizes.

3. Results and discussion

In the previous work, we tracked the paths of fresh particles in the 2D CRDE, obtained their p–v and T–s diagrams, and calculated the CRDE thermodynamic efficiency.[18] Now we use the particle path tracking method to analyze new 2D and 3D CRDE. Their particle paths and thermodynamic processes are analyzed and compared. For convenient comparison, we choose the same chamber size in the 2D and 3D simulations. The radius of the 2D combustion chamber is 4.5 cm, and the length is 4.8 cm. While the average radius of the 3D combustion chamber is also 4.5 cm, length 4.8 cm, and chamber width is 1 cm. After the detonation wave propagates stably along the circumferential direction, we track a large number of particles, which are injected into the combustion chamber.

3.1. 2D particle path Analysis

In the 2D numerical simulation, the chamber width along the radial direction is assumed to be much smaller than the diameter and axial length, and then the flow-field can be approximated as a 2D cylindrical surface without thickness. To show it clearly, the cylindrical surface is unrolled in a rectangular plane. Figure 4 shows the distribution of the reaction process variable after the detonation has propagated in a stable manner. At this instant, a larger number of flow particles are injected into the head-end of the combustion chamber, and they are tracked until they are exhausted out of the exit.

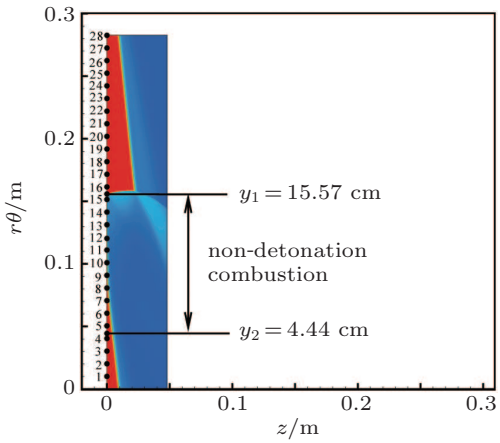


Fig. 4. (color online) Reaction process variable contour and initial positions of marked particles.

Figure 4 shows only 28 particle paths and thermodynamic processes. The initial positions of these particles are marked with "1, 2, ..., 28" sequentially. Most of the particles injected into the combustion chamber will be burned by the detonation wave, and the others will be burned by the high-temperature product in the flow field. In this 2D case, the particles, which are injected into the chamber between the lines $y_2 = 4.44$ cm and $y_1 = 15.57$ cm as shown in Fig. 4, are burned by the high-temperature product, and the others are burned by the detonation wave. In the present 2D chamber size, about 60.6% fresh

particles injected into the chamber are burned by the detonation wave. The pressure through the whole head end is less than the total pressure through the inlet (3 MPa), therefore the fresh particles can be injected at the whole head end.

Figure 5 shows the paths of the 28 particles from injection into the combustion chamber to their exhaustion from it. It is seen that the paths are generally along the axial direction no matter where their initial positions are. The particle paths have only small fluctuations along the circumferential direction, and the fluctuation of particle "19" is maximum, which is only 8.3% of the perimeter of the combustion chamber. The detonation wave, which propagates along the circumferential direction, has only a small effect on the flow particle's path.

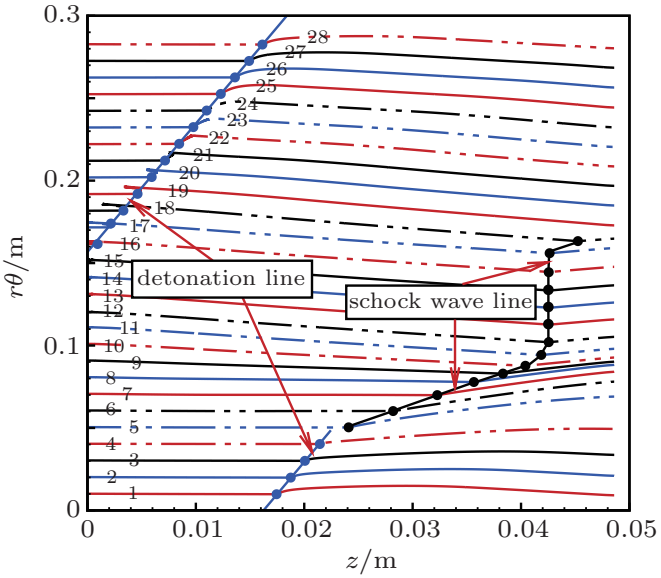


Fig. 5. (color online) Paths of 28 particles in 2D simulation.

After the particles are injected into the chamber, most of them encounter the detonation wave, and are burned instantaneously, such as particles "1–4" and "16–28" as shown in Fig. 5. When they encounter the detonation wave, their paths are deflected at that instant, as shown the intersection points between the paths and the "detonation line" in Fig. 5. The others are burned by the high-temperature product between the fresh gas and the combustion product, such as particles "5–15". Therefore, flow particles are injected into the combustion chamber, burned by the detonation wave or the high-temperature product, and then rapidly ejected almost along the axial direction. These characteristics support that a CRDE can produce the great axial thrust. Particles "5–18" encounter the accompanying oblique shock wave and their paths are also deflected as shown by the intersection points between the paths and the "shock wave line" in Fig. 5.

Figure 6 shows the p–v and T–s diagrams of the marked 28 particles. It is seen that most of the particles are compressed first by the gas mixture in the combustion chamber, after they have been injected into the chamber. In this process, their pressure and temperature increase to 3.8 atm and 590 K respectively. Then the fresh particles are burned by the detonation or the high-temperature product. As shown in Fig. 6, the pressure, temperature, and entropy increment increase rapidly, and the specific volume decreases slightly, when the detonation occurs. However in the process of the high-temperature product combustion, the specific volume, temperature, and entropy increment increase obviously, and the pressure decreases slightly (similar to the constant-pressure combustion). The process of high-temperature product combustion is completely consistent with the theory process of the deflagration. There is expansion process after the detonation, and the entropy increment increases slightly in the expansion process. There is no obvious expansion phenomenon after the high-temperature product combustion. The particles encounter the oblique shock wave, causing the fluctuations of p–v and T–s curves. However, their general trends are not changed. Therefore the accompanying oblique shock wave has no obvious effect on the performance of CRDE.

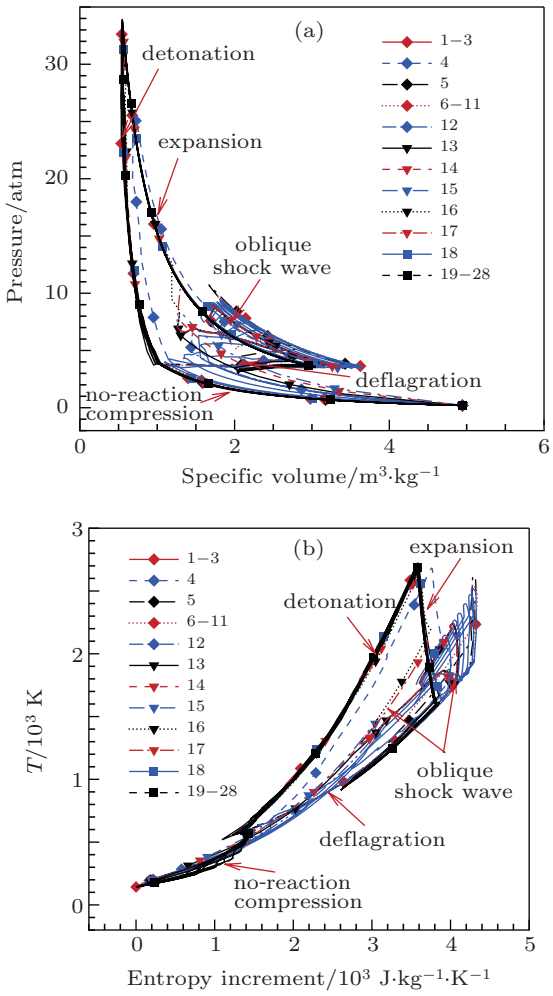


Fig. 6. (color online) Curves of p–v (a) and T–s (b) of the marked 28 particles in 2D simulation.

3.2. 3D particle path Analysis

Generally, the flow field of 3D CRDE is more complicated than that of 2D. After the rotating detonation stably propagates dynamically, a larger number of the flow particles are tracked in the combustion chamber. Their initial positions are different along the circumferential direction from the radial direction. To show clearly, only the paths of finite particles and thermodynamic processes are shown. Figure 7 shows the distribution of the reaction process variable on the head end and the initial positions of the marked particles. Their initial positions are marked with "$a1,\ldots,a17$", "$b1,\ldots,b17$", and "$c1,\ldots,c17$" on the inner annulus, outer annulus, and mid annulus respectively.

In the flow field of the rotating detonation, the pressure after the detonation wave is very high. When the pressure at the head end is larger than the inlet total pressure, the fresh gas mixture cannot be injected into the chamber, and this area is called no-injection area. The no-injection area proportion is defined as the ratio of the length of no-injection area to the perimeter of the corresponding annulus. The non-detonation proportion is defined as the ratio of the fresh particles burned by the high-temperature product to the total fresh particles injected into the chamber. As the chamber width increases, the flow field along the radial direction becomes more and more different.[19] The no-injection area proportion, non-detonation proportion and detonation front height are all different on the different annuli. Table 1 shows the no-injection area proportions, non-detonation proportions, and detonation front heights on the inner, mid, and outer annuli. As the radius of the annulus increases, the no-injection area proportions increases, the non-detonation proportion decreases, and the detonation height decreases. In the flow field of 3D CRDE, the non-detonation proportion is less than in the 2D flow field. The effects of the inner wall and outer wall on the detonation flow field in the 2D simulation are not considered, therefore the non-detonation proportion is overestimated.

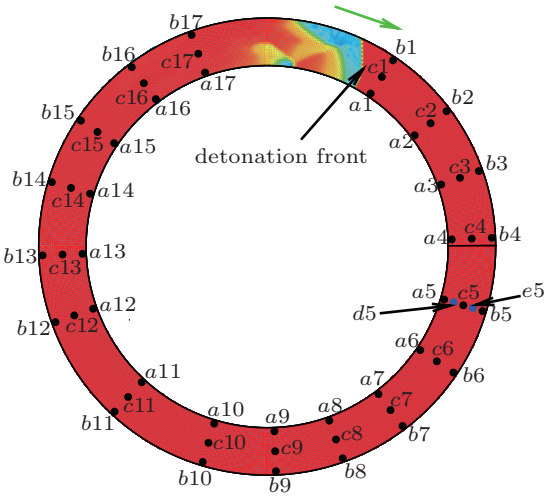


Fig. 7. (color online) Distributions of the reaction process variable at the head end and initial positions of marked particles in 3D simulation.

Table 1. No-injection area proportions, non-detonation proportions, and detonation heights on the different annuli.

	Outer annulus	Mid annulus	Inner annulus
No-injection area proportion/%	4.7	2.4	1.9
Non-detonation proportion/%	3.1	12.7	22.7
Detonation height/mm	25.1	26.0	31.2

Figure 8 shows the path fluctuations of the flow particles along the circumferential direction, whose initial positions are on the middle annulus, marked with "$c1,\ldots,c17$" in Fig. 7. Particles "$c1,\ldots,c16$" encounter the detonation wave after they have been injected into the combustion chamber, and their paths are deflected at that instant. Particle "$c17$" is burned by the high-temperature product in the flow field, and its path does not deflect in the combustion process. Particles "$c1$" and "$c17$" encounter the oblique shock wave, and their paths are deflected at that instant. In Fig. 8, the fresh particles cannot be injected into the chamber because of the high pressure after the detonation wave, which is between the lines $y_2 = 22.8$ cm and $y_1 = 23.4$ cm. The pressure increases again, which is caused by the shock wave reflection near the head end, thus the fresh particles cannot be injected into the area between the lines $y_1 = 23.4$ cm and $y_3 = 21.4$ cm either. The fresh particles, which are injected into the area between the lines $y_3 = 21.4$ cm and $y_2 = 22.8$ cm and between the lines $y_2 = 22.8$ cm and $y_4 = 21.1$ cm, are burned by the high-temperature product. In this mid annulus, about 12.7% fresh particles are burned by the high-temperature product. As shown in Fig. 8, similar to the 2D results, the path fluctuation along the circumferential direction is very small, and the fluctuation is only less than 12.6% of the fluctuation on the perimeter of the middle annulus. When the particle initial position and the detonation wave are closer to each other, the fluctuation of its path along the circumferential direction is more obvious.

Figure 9 shows the variations of path, pressure, and temperature of particle "$a2$" with axial distance. The particle pressure and temperature increase rapidly, and its path is deflected when it encounters the detonation wave. After encountering the detonation wave, the pressure decreases rapidly until it in-

creases suddenly again because of the reflected shock wave after the detonation wave. In the 3D CRDE chamber, when the chamber width is larger, the radial phenomenon is more and more obvious, and shock wave reflections between the inner wall and outer wall can be seen clearly. The second pressure peak in Fig. 9 is just caused by the reflected shock wave. The influences of various chamber geometries on the shock wave reflections near the head end of CRDE have been investigated in detail.[19]

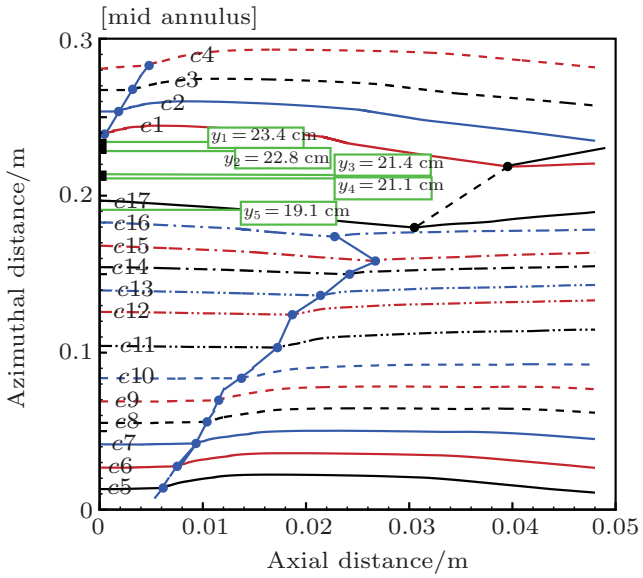


Fig. 8. (color online) Paths of particles on the middle annulus.

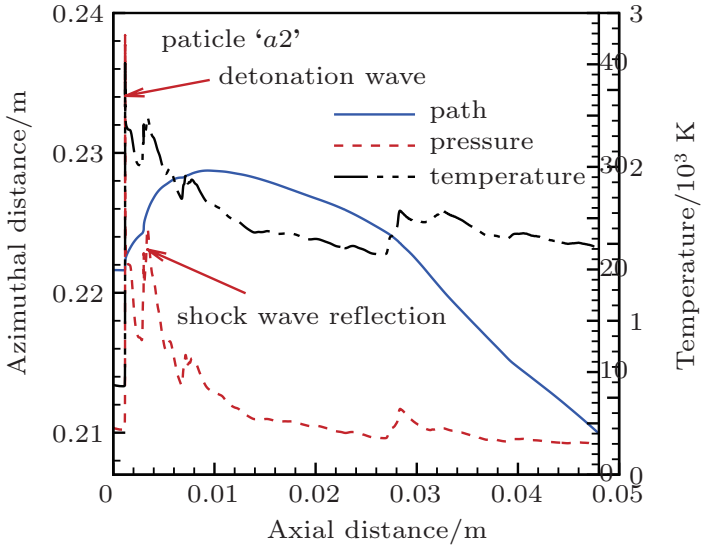


Fig. 9. (color online) Path, pressure, and temperature of particle "$a2$".

Now we look into the paths of the particles in detail, whose initial positions are different along the radial direction. Figures 10 and 11 show the path histories along the circumferential direction and radial direction, whose initial positions are marked with "$a5, d5, c5, e5, b5$" in Fig. 7. The path variations along the circumferential direction of the five particles, whose initial positions are on different annuli, are almost the same. When the particles encounter the detonation wave, their paths are deflected. Then the particles follow the detonation wave until the circumferential velocities decrease to zero, where their movement directions are changed again. The path fluctuations along the radial direction are not obvious as shown in Fig. 11. However the times of flowing out from the chamber are very greatly different. Figure 12 shows the axial velocities of the five particles, whose initial positions are on the different annuli. It is seen that the axial velocity of the particle near the outer annulus is smaller than near the inner annulus. Therefore the particle, whose initial position is near the outer annulus, needs a longer time to flow out from the combustion chamber than near the inner annulus. Near the head end, the detonation on the outer wall is stronger than on the inner wall, therefore the average pressure near the outer wall is higher than near the inner wall, and the axial velocity near the inner wall is bigger than near the outer wall.

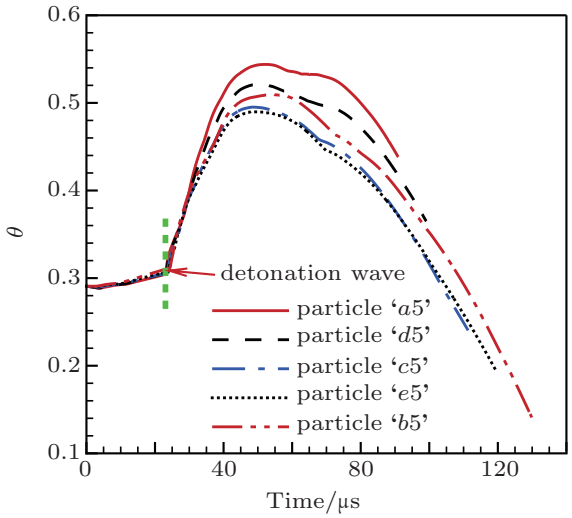


Fig. 10. (color online) Paths along circumferential direction.

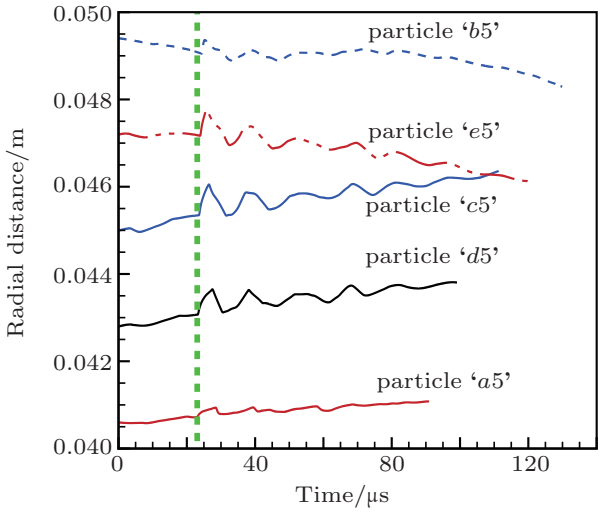


Fig. 11. (color online) Paths along radial direction.

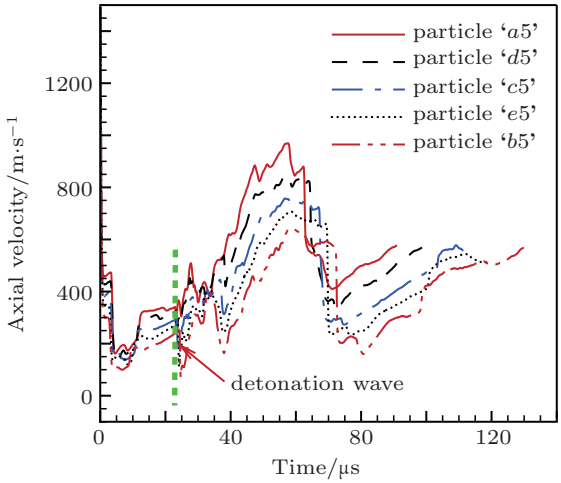


Fig. 12. (color online) Axial velocities of the five particles with initial positions on the different annuli.

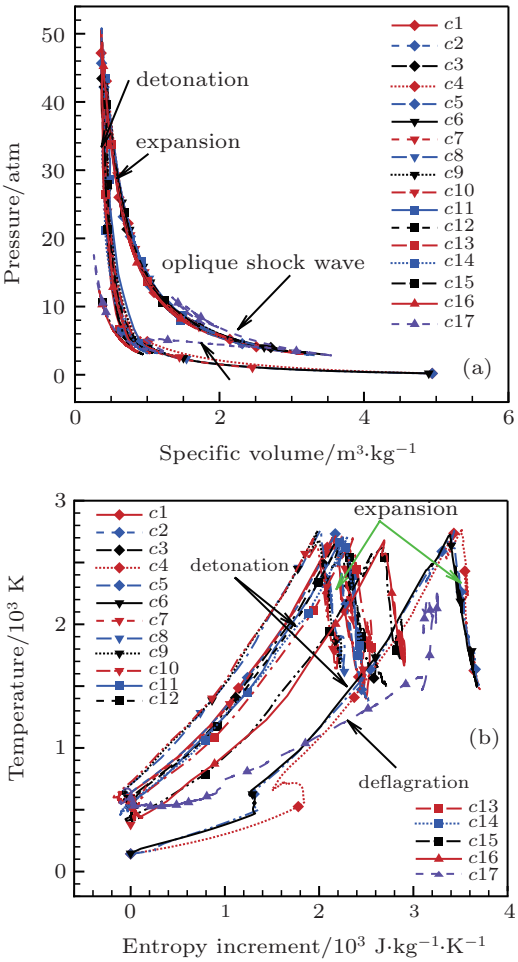


Fig. 13. (color online) (a) p–v and (b) T–s curves of particles, whose initial positions are on the mid annulus.

Figure 13 shows the p–v and T–s curves of 17 particles, whose initial positions are on the mid annulus marked with "$c1,\ldots,c17$" in Fig. 7. Particle "$c17$" is burned by the high-temperature product in the flow field. In this process, pressure decreases slightly (similar to the constant-pressure combustion), and the specific volume, temperature, and entropy increment increase obviously. Particles "$c1,\ldots,c16$" are burned by the detonation wave, and their thermodynamic processes are consistent. In the detonation process, the specific volume decreases slightly (similar to the constant-volume combustion), and the pressure, temperature, and entropy increment increase obviously. The pressure and temperature at the head end are set to be some values respectively, according to the relationship between the inlet stagnation pressure and the flow pressure at the head end,[19] therefore the initial pressures and temperatures of particles for p–v and T–s curves are different because of their different initial positions along the circumferential direction. However the net entropy increment and temperature increment are consistent in the detonation process.

3.3. Comparison between 2D and 3D results

Figure 14 shows the path comparisons of 2D (particles marked with "3, 12, 19, 23, 27" in Fig. 4) with 3D (particles marked with "$c3, c6, c9, c11, c17$" in Fig. 7) simulations, and the initial positions of these particles have a similar distance away from the detonation wave front. Particles "$c3, c6, c9, c11$" in 3D flow field and particles "19, 23, 27, 3" in 2D flow field are burned by the detonation wave, and particle "$c17$" in 3D flow field and particle "12" in 2D flow field are burned by the high-temperature product. The fluctuant trend along the circumferential direction of the 3D path is coincident with the 2D path, however the deflection of the 3D path is more gentle than that of the 2D path. In the 3D CRDE, the flow field of the rotating detonation interacts and couples with those on the different annuli, therefore the flow field parameters on the 3D mid annulus are different from those in the 2D flow field under the same chamber size. For example, in the 2D CRDE, the fresh particles can be injected into the chamber on the whole head end, and 39.4% fresh particles will be burned by the high-temperature product in the flow field. However on the mid annulus of the 3D CRDE, the fresh particles cannot be injected into the chamber in a small area on the head end because of the high pressure after the detonation wave, and the no-injection length is about 2.4% of the perimeter of the mid annulus. About 12.7% fresh particles will be burned by the high-temperature product in the flow field on this annulus.

Pressure as a function of specific volume is defined by the p–v curve, which represents the mechanical work of the thermodynamic process. Temperature as a function of the entropy increment is defined by the T–s curve, which represents the heat release of the thermodynamic process. There are three kinds of models to describe the thermodynamic process of the detonation. They are ideal Humphrey, F–J, and ZND cycle models respectively. In the Humphrey cycle model, the detonation is approximated to the constant-volume combustion, and then isentropic expansion occurs. According to the C–J theory of detonation, chemical reactions are modeled as a heat release in an infinitely thin zone, where the detonation

wave and induced shock wave fronts coincide together. The C–J theory does not consider the detonation wave structure. The F–J cycle[26,27] is just based on the C–J theory to describe the thermodynamic process of detonation. In the F–J cycle, the heat addition process is along the Rayleigh line from the initial point to the C–J point, and the isentropic expansion occurs after the detonation as shown in Fig. 15(a). Subsequent to the C–J theory, Zel'dovich, von Neumann and Doring independently developed a more appropriate theory, now known as the ZND model.[28] In this theory, the propagating detonation wave consists of an induced shock wave that raises the initial state to the von Neumann spike, followed by an induction zone and a reaction zone. However, unlike the C–J theory where the heat release occurs instantly, the ZND theory allows the heat release to occur from the von Neumann spike to the C–J point along the Rayleigh line as shown in Fig. 15(a).

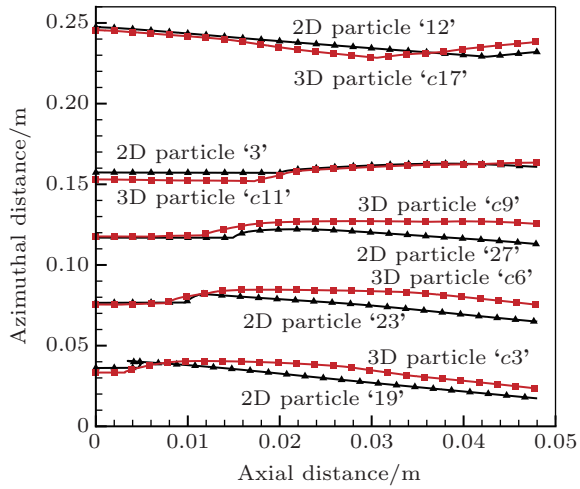


Fig. 14. (color online) Comparison of path between 2D and 3D simulations.

Indeed, the ideal F–J and ZND cycles include only the detonation compression, combustion, and isentropic expansion processes. Therefore, we also consider the corresponding processes to compare with the numerical simulations. In the 2D and 3D numerical simulations, the particle pressure and temperature increase to 3.8 atm and 590 K respectively before the detonation occurring. According to this initial condition, the thermodynamic processes of the three ideal detonation cycle models are derived theoretically. Figure 15 shows thermodynamic curves comparison of the 2D particle, 3D particle on the different annuli, ideal Humphrey model, F–J model, and ZND model.

Although both p–v and T–s curves are similar for 2D and 3D cases, there exist several small differences between them. The p–v curves show that the specific volume decreases slightly during the actual detonation, which is different from the constant-volume Humphrey cycle. The T–s curves show that the entropy increment increases slightly in the actual expansion process, not entirely isentropic like the ideal cycles, which is caused by the non-adiabatic movement process. The 3D detonation wave is more complex than the 2D detonation wave. The transverse waves exist only in the axial direction in the 2D detonation, however the transverse waves exist both in the axial direction and in the radial direction in the 3D detonation. Therefore the maximum pressure in the 3D p–v curve is higher than in the 2D p–v curve. The maximum entropy increment in the 3D T–s curve is slightly smaller than in the 2D T–s curve, and the maximum temperature in the 3D T–s curve is slightly higher than in the 2D T–s diagram.

As shown in Fig. 15, the numerical thermodynamic processes are qualitatively consistent with those obtained from the ideal models. The F–J cycle does not consider the compression process of the induced shock wave, while the ZND cycle overestimates this process. Therefore the p–v and T–s diagrams of the numerical simulations are right in between the ideal F–J cycle and ideal ZND cycle. The maximum pressure, entropy increment, and temperature in simulations are all smaller than those in the F–J and ZND cycles.

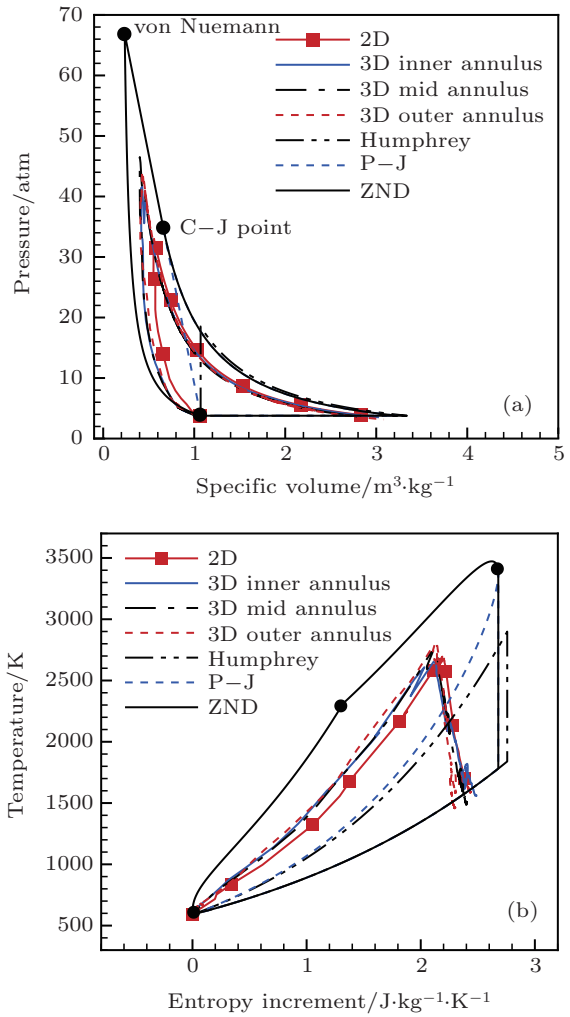


Fig. 15. (color online) Comparisons of the p–v (a) and T–s (b) curves from the 2D and 3D numerical simulation, the ideal Humphrey model, F–J model, and ZND model.

The thermal efficiency is defined as the ratio of the cycle

net mechanical work to the absorbed heat. The net mechanical work and the absorbed heat can be calculated through the p–v and T–s curves in Fig. 15. Table 2 shows the net mechanical work and thermal efficiencies of 2D particle and 3D particle on the inner, mid, and outer annuli, Humphrey, F–J, and ZND cycle models. The net work and thermal efficiency are slightly smaller in 2D simulation than in 3D simulation. In the 3D CRDE, as the radius of the annulus increases, the net mechanical work is almost constant, and the thermal efficiency increases. The numerical thermal efficiencies are larger than in F–J cycle model, and much smaller than in ZND cycle model. That is because the compression process of the induced shock wave is overestimated in the ZND cycle model, therefore the net mechanical work in the ZND cycle model is much larger than in the actual detonation cycle model.

Table 2. Comparisons of net mechanical work and thermal efficiency among different models.

	2D	3D-inner	3D-mid	3D-outer	Humphrey	F–J	ZND
Net mechanical work/(MJ/kg)	1.2	1.5	1.5	1.5	1.0	1.1	3.1
Thermal efficiency/%	30.9	32.5	34.6	35.3	24.2	27.8	51.5

4. Conclusions

(i) The flow field parameters on the 3D mid annulus are different from those in the 2D flow field under the same chamber size. In the 2D CRDE, fresh particles can be injected into the chamber through the whole head end, and 39.4% fresh particles will be burned by the high-temperature product in the flow field. However on the mid annulus of the 3D CRDE, the fresh particles cannot be injected into the chamber in the 2.4% area on the head end because of the high pressure after the detonation wave, and about 12.7% fresh particles will be burned by the high-temperature product. As the radius of the annulus increases, the no-injection area proportion increases, the non-detonation proportion decreases, and the detonation height decreases. In the 3D CRDE flow field, the non-detonation proportion is less than in the 2D flow field.

(ii) In the 2D and 3D CRDE, the paths of the flow particles have only a small fluctuation in the circumferential direction. Flow particles are injected into the combustion chamber, burned by the detonation wave or the high-temperature product, and then rapidly ejected almost along the axial direction. When the flow particles encounter the detonation wave or the oblique shock wave, their paths are deflected. The fluctuant trend along the circumferential direction of the 3D path is coincident with that of the 2D path, however the deflection of the 3D path is more gentle than that of the 2D path.

(iii) The numerical thermodynamic cycle processes are qualitatively consistent with the three ideal models, and they are right in between the ideal F–J cycle and ideal ZND cycle. The net mechanical work and thermal efficiency are slightly smaller in 2D simulations than in 3D simulations. In the 3D CRDE, as the radius of the annulus increases, the net mechanical work is almost constant, and the thermal efficiency increases. The numerical thermal efficiencies are larger than in F–J cycle model, and much smaller than in ZND cycle model.

References

[1] Huang Y, Ji H and Lien F S 2012 *Chin. Phys. Lett.* **29** 114701
[2] Han X, Zhou J and Lin Z Y 2012 *Chin. Phys. B* **21** 124702
[3] Shen H, Liu K X and Zhang D L 2011 *Chin. Phys. Lett.* **28** 124705
[4] Wolanski P 2013 *Proc. Combust. Inst.* **34** 125
[5] Lu F K, Braun E M, Massa L and Wilson D R 2011 *AIAA* **2011** 6043
[6] Voitsekhovskii B V 1959 *Doklady Akademii Nauk SSSR* **129** 1254
[7] Adamson T C Jr and Olsson G R 1967 *Astronautica Acta* **14** 405
[8] Nicholls J A, Cullen R E and Ragland K W 1966 *J. Spacecraft Rockets* **3** 893
[9] Bykovskii F A, Zhdan S A and Vedernikov E F 2006 *J. Propul. Power* **22** 1204
[10] Zhdan S A, Bykovskii F A and Vedernikov E F 2007 *Combust. Expl. Shock Waves* **43** 449
[11] Kindracki J, Wolanski P and Gut Z 2011 *Shock Waves* **21** 75
[12] Davidenko D M, Gokalp I and Kudryavtsev A N 2008 *AIAA* **2008** 2680
[13] Eude Y, Davidenko D M and Gokalp I 2011 *AIAA* **2011** 2236
[14] Schwer D A and Kailasanath K 2012 *AIAA* **2012** 0617
[15] Shao Y T and Wang J P 2010 *Chin. Phys. Lett.* **27** 034705
[16] Shao Y T and Wang J P 2010 *Chin. J. Aeronaut.* **23** 647
[17] Shao Y T, Liu M and Wang J P 2010 *Combust. Sci. Technol.* **182** 1586
[18] Zhou R and Wang J P 2012 *Combust. Flame* **159** 3632
[19] Zhou R and Wang J P 2013 *Shock Waves* **23** 461
[20] Liu S J, Lin Z Y and Sun M B 2011 *Chin. Phys. Lett.* **28** 094704
[21] Hishida M, Fujiwara T and Wolanski P 2009 *Shock Waves* **19** 1
[22] Uemura Y, Hayashi A K, Asahara M, Tsuboi N and Yamada E 2013 *Proc. Combust. Inst.* **34** 1981
[23] Korobeinikov V P and Levin V A 1972 *Astronautica Acta* **17** 529
[24] Balsara D S and Shu C W 2000 *J. Comput. Phys.* **160** 405
[25] Shu C W and Osher S 1989 *J. Comput. Phys.* **83** 32
[26] Wintenberger E and Shepherd J E 2006 *J. Propul. Power* **22** 694
[27] Fickett W and Davis W C 2001 *Detonation Theory and Experiment* **2** 35
[28] Heiser W H and Pratt D T 2002 *J. Propul. Power* **18** 68